1 **Title:** Characterization of extracellular vesicles and artificial nanoparticles with four orthogonal
2 single-particle analysis platforms

3

4 **Authors:**
5 Emily R. Mallick[1,#], emilymallick@gmail.com
6 Tanina Arab[1,#] ORCID 0000-0003-4485-1096, tarab1@jhu.edu
7 Yiyao Huang[1] ORCID 0000-0003-1749-963X, yiyaohuang@jhu.edu
8 Liang Dong[2] ORCID 0000-0001-7689-3237, ldong4@jhmi.edu
9 Zhaohao Liao[1], zliao@jhmi.edu
10 Zezhou Zhao[1] ORCID 0000-0003-4792-6073, zach.zhao621@gmail.com
11 Barbara Smith[3], bsmit112@jhmi.edu
12 Norman J. Haughey[4] ORCID 0000-0001-5194-4122, nhaughe1@jhmi.edu
13 Kenneth J. Pienta[2] ORCID 0000-0002-4138-2186, kpienta1@jhmi.edu
14 Barbara S. Slusher[4,5] ORCID 0000-0001-9814-4157, bslusher@jhmi.edu
15 Patrick M. Tarwater[6] ORCID 0000-0002-6791-1090, tarwater@jhu.edu
16 Juan Pablo Tosar[7,8] ORCID 0000-0002-2021-2479, jptosar@pasteur.edu.uy
17 Angela M. Zivkovic[9] ORCID 0000-0002-2828-7862, amzivkovic@ucdavis.edu
18 Wyatt N. Vreeland[10] ORCID 0000-0003-0524-8403, wyatt.vreeland@nist.gov
19 Michael E. Paulaitis[11] ORCID 0000-0002-9628-1091, michaelp@jhmi.edu
20 Kenneth W. Witwer[1,4,*] ORCID 0000-0003-1664-4233, kwitwer1@jhmi.edu

21

22 **Author Information:**
23 [1]Department of Molecular and Comparative Pathobiology, Johns Hopkins University School of
24 Medicine, Baltimore, MD, US
25 [2]Department of Urology, Johns Hopkins University School of Medicine, Baltimore, MD, US
26 [3]Department of Cell Biology, Johns Hopkins University School of Medicine, Baltimore, MD,
27 US
28 [4]Department of Neurology, Johns Hopkins University School of Medicine, Baltimore, MD, US
29 [5]Johns Hopkins Drug Discovery, Johns Hopkins University School of Medicine, Baltimore,
30 MD
31 [6]Department of Epidemiology, Johns Hopkins University Bloomberg School of Public Health,
32 Baltimore, MD, US
33 [7]Faculty of Science, Universidad de la República, Montevideo, Uruguay
34 [8]Functional Genomics Unit, Institut Pasteur de Montevideo, Montevideo, Uruguay
35 [9]Department of Nutrition, University of California Davis, Davis, CA, US
36 [10]Bioprocess Measurement Group, National Institute of Standards and Technology,
37 Gaithersburg, MD, US
38 [11]Center for Nanomedicine at the Wilmer Eye Institute, Johns Hopkins University School of
39 Medicine, Baltimore, MD, US

40

41   #These authors contributed equally to this work

42

43   ***Corresponding Author:**

44   Kenneth W. Witwer, PhD

45   733 North Broadway

46   Miller Research Building, Room 827

47   Baltimore, MD 21205

48   Phone: 1-410-955-9770

49   Fax: 1-410-955-9823

50   Email: kwitwer1@jhmi.edu

51

55

56

ABSTRACT

We compared four orthogonal technologies for sizing, counting, and phenotyping of extracellular vesicles (EVs) and synthetic particles. The platforms were: single-particle interferometric reflectance imaging sensing (SP-IRIS) with fluorescence, nanoparticle tracking analysis (NTA) with fluorescence, microfluidic resistive pulse sensing (MRPS), and nanoflow cytometry measurement (NFCM). Results were compared with standard EV characterization techniques such as transmission electron microscopy (TEM) and Western blot (WB). EVs from the human T lymphocyte line H9 (high CD81, low CD63) and the promonocytic line U937 (low CD81, high CD63) were separated from culture conditioned medium (CCM) by differential ultracentrifugation (dUC) or a combination of ultrafiltration (UF) and size exclusion chromatography (SEC) and characterized per MISEV2018 guidelines. Mixtures of synthetic particles (silica and polystyrene spheres) with known sizes and/or concentrations were also tested. MRPS and NFCM returned similar particle counts, while NTA detected counts approximately one order of magnitude lower for EVs, but not for synthetic particles. SP-IRIS events could not be used to estimate particle concentrations. For sizing, SP-IRIS, MRPS, and NFCM returned similar size profiles, with smaller sizes predominating (per power law distribution), but with sensitivity typically dropping off below diameters of 60 nm. NTA detected a population of particles with a mode diameter greater than 100 nm. Additionally, SP-IRIS, MRPS, and NFCM were able to identify at least three of four distinct size populations in a mixture of silica or polystyrene nanoparticles. Finally, for tetraspanin phenotyping, the SP-IRIS platform in fluorescence mode and NFCM were able to detect at least two markers on the same particle. Based on the results of this study, we can draw conclusions about existing single-

3

79   particle analysis capabilities that may be useful for EV biomarker development and mechanistic

80   studies.

81

82

83   **INTRODUCTION**

84

85   Classification of extracellular vesicles (EVs) into subtypes has been proposed based on size,

86   biogenesis pathway, separation procedure, cellular or tissue origin, and function, among others

87   [1–6]. However, reproducible classification of EV subtypes will require single-particle

88   characterization techniques including phenotyping by surface molecules or molecular signatures

89   [7,8]. In this sense, current knowledge of EV subtypes could be compared with knowledge of

90   immune cells in the 1970s and early 1980s. Around that time, multiplexed flow cytometry

91   capabilities and cell sorting were developed, allowing more precise identification,

92   characterization, and molecular and functional profiling of immune cell subsets [9]. Single-

93   particle technologies for much smaller biological entities will be needed to divide heterogeneous

94   EV populations into well-defined and easily recognized subgroups.

95

96   In this study, we evaluated several particle types and single-particle characterization platforms.

97   For input, we used a selection of biological and synthetic particles. EVs were separated from

98   culture medium of H9 T lymphocytic cells and U937 promonocytic cells using several methods.

99   These two cell lines were chosen because they display distinct tetraspanin levels. Specifically,

100   H9 have high CD81 and low CD63 levels, while U937 produce little CD81 but abundant CD63.

101   Mixtures of distinct sizes of synthetic silica and polystyrene beads were also tested. The

102   technology platforms (Text Box 1) were: single-particle interferometric reflectance imaging

103   sensing (SP-IRIS, NanoView) [10,11] with fluorescence, nanoparticle tracking analysis (NTA,

104   ParticleMetrix) [12–14] with fluorescence, microfluidic resistive pulse sensing (MRPS,

105   Spectradyne) [14,15], and nanoflow cytometry measurement (NFCM, NanoFCM) [16,17].

5

106

Text Box 1: Evaluated Technologies

Single-particle interferometric reflectance imaging sensing (SP-IRIS) captures particles (*e.g.* EVs) onto a chip by affinity reagents, usually antibodies, to surface antigens. Particles are imaged by interferometric reflectance for sizing and counting, and fluorescence detection may be done for up to three channels for surface antigens or internal molecules following fixation and permeabilization. Website for the platform we used: https://www.nanoviewbio.com/

Nanoparticle tracking analysis (NTA) is an optical method to track single particles and assign sizes and counts. Measuring Brownian motion allows calculation of a hydrodynamic sphere-equivalent radius of each tracked particle. Additionally, fluorescence filters can be used for detection of particle-associated fluorescence moieties channels. Website for the platform we used: https://www.particle-metrix.de/en/particle-metrix

Microfluidic resistive pulse sensing (MRPS) counts and sizes particles as they pass through a pore between microfluidic chambers. Occlusion of the pore results in a measurable change in electrical signal (defining an event) that is proportional to the volume of the particle. Often, this technique uses different disposable cartridge pore sizes to detect particle populations within specific size ranges. As a non-optical technology, fluorescence detection is not available. Website for the platform we used: https://nanoparticleanalyzer.com/

Nanoflow cytometry measurement (NFCM) is a flow-based technique that detects nano-sized particles by scatter and/or fluorescence. Compared with traditional flow cytometry, a smaller flow channel reduces background signal, and lower system pressure increases dwell time of particles for enhanced signal integration. Website for the platform we used: http://www.nanofcm.com/products/flow-nanoanalyzer

---

107

108   **MATERIALS AND METHODS**

109

110   *Please see Table 1 for manufacturer, part number, and (where applicable) dilution of reagents.*

111   ***Certain commercial equipment, instruments, and reagents are identified in this paper to foster***

112   ***understanding. Such identification does not imply recommendation or endorsement by the***

113   ***National Institute of Standards and Technology or any other entity, nor does it imply that the***

114   ***materials or equipment identified are necessarily the best available for the purpose.***

115

116   **Particle Preparation:** Human cells lines H9 (T lymphocytic) and U937 (pro-monocytic) were

117   obtained from the American Type Culture Collection (ATCC). Cells were maintained in Roswell

118   Park Memorial Institute (RPMI) 1640 Medium supplemented with either replete or EV-depleted

119   10% heat-inactivated fetal bovine serum, with 1% HEPES buffer, 1% Penicillin-Streptomycin,

120   and 1% L-Glutamine. Cells were cultured at 37°C in 5% CO_2. Silica spheres (SS) were obtained

121   from NanoFCM (Nottingham, England) as a premixed combination of diameters 68 nm, 91 nm,

122   113 nm, and 151 nm. Individual polystyrene spheres (PS) were purchased at diameters 70 nm, 90

123   nm, 122 nm, and 152 nm. Equal concentrations (1×10^{12} particles/mL) of beads were mixed.

124

125   **Size Exclusion Chromatography (SEC):** 60 mL of conditioned culture medium (CCM) from

126   each cell line was centrifuged at $1,000 \times g$ for 5 minutes at 4°C to remove cells and cellular

127   debris. 3 kDa molecular weight cut off (MWCO) Centricon Plus-70 centrifugal filters (Millipore

128   Sigma) were used to concentrate the initial volume to 1.5 mL. Size exclusion chromatography

129   (SEC) was done with qEV Automated Fraction Collectors (AFC; Izon Science, Cambridge, MA)

130   and qEV original 70 nm columns (Izon Science, Cambridge, MA). Columns were left at room

7

131   temperature for 30 minutes and washed with phosphate-buffered saline (PBS). EVs were loaded

132   onto the column, and 0.5 mL fractions were collected by adding additional PBS to the column.

133   EV enriched fractions (SEC; fractions 7-9) were pooled and further concentrated using 3 kDa

134   MWCO Amicon Ultra-15 Centrifugal Filters to a final volume of 1 mL. 50 µL aliquots were

135   stored at -20°C for downstream assays.

136

137   **Differential Ultracentrifugation (dUC):** 60 mL of CCM from each cell line was centrifuged at

138    $1,000 \times g$ for 5 minutes at 4°C to remove cells and cellular debris and $2,000 \times g$ for 10 minutes at

139   4°C to remove additional debris. The supernatant was transferred to polypropylene thin-wall

140   ultracentrifugation (UC) tubes and centrifuged at $10,000 \times g$ for 30 minutes at 4°C using a

141   swinging bucket rotor (Thermo Scientific rotor model AH-629, k-factor 242, acceleration and

142   deceleration settings of 9) to pellet large EVs. Supernatant was transferred into new

143   polypropylene thin wall UC tubes and centrifuged at $100,000 \times g$ for 70 minutes at 4°C using the

144   same swinging bucket rotor. The 100K pellets containing small EVs were resuspended in 1 mL

145   of PBS, vigorously vortexed, and placed on ice for 20 minutes. 50 µL aliquots were stored at -

146   20°C for downstream assays.

147

148   **Transmission Electron Microscopy (TEM)**: 10 µL freshly thawed aliquots were adsorbed to

149   glow-discharged carbon-coated 400 mesh copper grids by flotation for 2 minutes. Grids were

150   quickly blotted and rinsed by flotation on 3 drops (1 minute each) of 1× Tris-buffered saline.

151   Grids were negatively stained in 2 consecutive drops of 1% uranyl acetate (UAT)

152   with tylose (1% UAT in deionized water (dIH$_2$O), double filtered through a 0.22 µm filter),

153   blotted, then quickly aspirated to cover the sample with a thin layer of stain. Grids were imaged

154   on a Hitachi 7600 TEM operating at 80 kV with an AMT XR80 CCD (8 megapixel). SS and PS

155   were absorbed to grids as above, but with initial flotation for 5 minutes and imaging on a Phillips

156   CM-120 TEM operating at 80 kV with an AMT XR80 CCD (8 megapixel).

157

158   **Western Blot (WB):** H9 and U937 cell pellets and isolated EVs were lysed in 1×

159   radioimmunoprecipitation assay buffer (RIPA) supplemented with protease inhibitor cocktail.

160   Protein quantification of cell and EV lysates was done using a bicinchoninic acid assay (BCA)

161   (Pierce BCA Protein Assay Kit). 5 μg of lysates were resolved using a 4% to 15% Criterion

162   TGX Stain-Free Precast gel, then transferred onto an Immuno-Blot PVDF membrane. Blots were

163   probed using primary antibodies in PBS-T and 5% Blotting Grade Blocker. Primary antibodies

164   included anti-CD81, anti-CD63, anti-CD9, anti-TSG101, anti-BiP/GRP78, and anti-GM130.

165   Rabbit anti-mouse IgGk BP-HRP and Mouse anti-rabbit IgGk BP-HRP were used as secondary

166   antibodies. SuperSignal West Pico PLUS Chemiluminescent Substrate was used for detection

167   and blots were visualized with an iBright Western Blot (Thermo Fisher, Waltham, MA) imaging

168   system.

169

170   **Single Particle Interferometric Reflectance Imaging (SP-IRIS):** Measurements were

171   performed largely as described previously [18,19]. 35 μL of H9 and U937 EVs isolated by SEC

172   or dUC were diluted 1:1 in incubation buffer (IB) and incubated at room temperature

173   on ExoView R100 (NanoView Biosciences, Brighton, MA) chips printed with anti-human CD81

174   (JS-81), anti-human CD63 (H5C6), anti-human CD9 (HI9a), and anti-mouse IgG1 (MOPC-21).

175   After incubation for 16 hours, chips were washed with IB 4 times for 3 minutes each under

176   gentle horizontal agitation at 500 rpm. Chips were then incubated for 1 hour at room temperature

9

177   with a fluorescent antibody cocktail of anti-human CD81 (JS-81, CF555), anti-human CD63

178   (H5C6, CF647), and anti-human CD9 (HI9a, CF488A) at a dilution of 1:1200 (v:v) in a 1:1 (v:v)

179   mixture of IB and blocking buffer. The buffer was then exchanged to IB only, followed by 1

180   wash with IB, 3 washes with wash buffer, and 1 wash with rinse buffer (3 minutes each at 500

181   rpm). Chips were immersed twice in rinse buffer for approximately 5 seconds each and removed

182   at a 45-degree angle to allow the liquid to vacate the chip. All reagents and antibodies were

183   supplied by NanoView Biosciences (Brighton, MA, Cat #EV-TETRA-C). Both SS and PS were

184   diluted in dIH$_2$O to load 10,000 particles, nominally, per antibody capture spot on

185   the ExoView chips. 35 µL of diluted spheres were incubated on ExoView chips and allowed to

186   fully dry. All chips were imaged in the ExoView scanner (NanoView Biosciences, Brighton,

187   MA) by interferometric reflectance imaging and fluorescent detection. Data were analyzed

188   using NanoViewer 2.8.10 Software (NanoView Biosciences). Fluorescent cutoffs were as

189   follows: CF555 channel 230, CF488 channel 475, CF647 channel 250 (biological particles) and

190   CF555 channel 675, CF488 channel 600, and CF647 channel 375 (SS and PS).

191

192   **Nanoparticle Tracking Analysis (NTA):** ZetaView QUATT-NTA Nanoparticle Tracking-

193   Video Microscope PMX-420 and BASIC NTA-Nanoparticle Tracking Video Microscope PMX-

194   120 (Particle Metrix, Inning am Ammersee, Germany) instruments were used for particle

195   quantification in both scatter and fluorescence (488 nm) modes. All calibration beads were

196   diluted using distilled water, and all samples were diluted in PBS to a final volume of 1 mL.

197   Calibration was done for both scatter and fluorescence measurements. For scatter-mode

198   calibration, 100 nm PS were diluted 1:250,000 (v:v). Capture settings were: sensitivity 65,

199   shutter 100, minimum trace length 10. Cell temperature was maintained at 25°C for all

200   measurements. For fluorescence calibration, 488 nm yellow-green FluoSpheres were diluted

201   1:250,000 (v:v), and both scatter and fluorescence were measured. Scatter was recorded as

202   above, and fluorescence was measured at sensitivity 80, shutter 100, and minimum trace length

203   15. For H9 and U937 EVs isolated by SEC or dUC, one cycle was performed by scanning 11 cell

204   positions. Capture was done at medium video setting corresponding to 30 frames per position.

205   PE-conjugated mouse anti-human CD81 and AF488-conjugated mouse anti-human CD63 were

206   used for fluorescence detection of EVs. Antibodies were mixed 1:9 (v:v) with PBS, incubated 2

207   hours at room temperature, and diluted to a final volume of 1 mL. For SS and PS mixtures,

208   samples were diluted such that at least 200 particles could be counted per frame. Technical

209   triplicates were measured for each sample. A washing step was done between each measurement

210   using dIH$_2$O. ZetaView Software 8.5.10 was used to analyze the recorded videos with the

211   following settings: minimum brightness 30, maximum brightness 255, minimum area 10, and

212   maximum area 1000. Supplementary Table 1 lists all antibodies tested with this platform.

213

214   **Microfluidic Resistive Pulse Sensing (MRPS):** Microfluidics resistive pulse sensing

215   measurements were conducted using the nCS1 instrument (Spectradyne, Torrance, CA) as

216   described previously [18]. Sample volumes of a few μL of H9 and U937 EVs isolated by SEC or

217   dUC were diluted with an equal volume of 1% polysorbate 20 (Tween 20) in 1× PBS (PBST)

218   and further diluted with 1× PBS, and loaded onto polydimethylsiloxane cartridges (diameter

219   range 65 nm to 400 nm). Approximately 5 μL of the diluted sample was used and about 25,000

220   events were recorded for each analyte. SS and PS were diluted 100-fold by volume in dIH$_2$O,

221   then 10-fold by volume with equal volumes of PBST and the remainder with 1× PBS and loaded

222   onto TS-400 polydimethylsiloxane cartridges. Approximately 3,000 events were obtained for

11

223   each SS and PS repeat. All acquired results were analyzed using the nCS1 Data Analyzer

224   (Spectradyne, Torrance, CA). For all samples, user-defined filtering was applied by defining 2D

225   polygonal boundaries based on transition time and diameter to exclude false positive signals,

226   similar to gating commonly used in analyzing flow cytometry data.

227

228

229   **Nano-Flow Cytometry Measurement (NFCM):** The nFCM flow nano-Analyzer was used to

230   measure concentration and size of particles following the manufacturer's instructions and as

231   described previously [20]. Briefly, two single photon-counting avalanche photodiodes (APDs)

232   were used for the simultaneous detection of side scatter (SSC) and fluorescence of individual

233   particles. The instrument was calibrated separately for concentration and size using 200 nm PE-

234   and AF488 fluorophore-conjugated PS beads and a Silica Nanosphere Cocktail, respectively.

235   20 μL of each EV preparation was incubated with 20 μL PE-conjugated CD81 and 5 μL AF488-

236   conjugated CD63 antibodies at 37°C for 30 minutes. After incubation, the mixture was washed

237   twice with PBS and centrifuged at 110,000 × g for 70 min at 4°C (TH-641 rotor, k-factor 114,

238   Thermo Fisher, using thin-wall polypropylene tubes with 13.2 ml capacity and acceleration and

239   deceleration settings of 9). The pellet was resuspended in 50 μL PBS. Events were recorded for 1

240   minute. Using the calibration curve, the flow rate and side scattering intensity were converted

241   into corresponding particle concentrations and size.

242
243

12

244 **Table 1**

Antibodies	Manufacturer	Cat #	Dilution
Primary Anti-CD81	Santa Cruz, Dallas, TX	sc-7637	1:500
Primary Anti-CD63	BD Pharmigen, San Diego, CA	556019	1:1000
Primary Anti-CD9	BioLegend, San Diego, CA	312102	1:1000
Primary Anti-TSG101	AbCam, Cambridge, MA	ab125011	1:1000
Primary Anti-BiP/GRP78	BD Pharmigen, San Diego, CA	619078	1:500
Primary Anti-GM130	AbCam, Cambridge, MA	ab52649	1:400
Secondary Mouse Anti-Rabbit IgG BP-HRP	Santa Cruz, Dallas, TX	sc-2357	1:5000
Secondary Rabbit Anti-Mouse IgGk BP-HRP	Santa Cruz, Dallas, TX	516102	1:5000
PE-Conjugated Mouse Anti-Human CD81	BD Biosciences, Franklin Lakes, NJ	555676	n/a
AF488-Conjugated Mouse Anti-Human CD63	Novus Biologicals, Littleton, CO	NBP2-42225	n/a
Reagents	**Manufacturer**	**Cat #**	
3K MWCO Centricon Plus-70	Millipore Sigma	UFC700308	
3K MWCO Amicon Ultra-15	Millipore Sigma	UFC900396	
Blotting Grade Blocker	Bio-Rad	170-6404	
Carbon Coated 400 Mesh Copper Grids	Electron Microscopy Science	CF400-Cu-UL	
Criterion TGX Stain-Free Precast Gel	Bio-Rad	5678084	
Distilled Water	Gibco	15230-162	
FluoSpheres Carboxylate-Modified Microspheres, 0.1 μm, Yellow Green Fluorescent	Thermo Scientific	F8803	
H9 Cell Line	American Type Culture Collection	HTB-176	
Heat-Inactivated Fetal Bovine Serum	GE Healthcare	SH30396.03	
Heat-Inactivated Fetal Bovine Serum, Exosome-Depleted	Gibco	A2720801	
HEPES buffer	Gibco	15630080	
Immuno-Blot PVDF Membrane	Bio-Rad	1620177	
L-Glutamine	Gibco	25030081	
Open-Top Thin Wall Ultra-Clear Tubes	Beckman Coulter	344091	
Penicillin-Streptomycin	Gibco	15140122	

13

Phosphatidylserine Beads	NanoFCM	S16M-Exo
Phosphate-Buffered Saline (PBS)	Gibco	14190-144
Pierce BCA Protein Assay Kit	Thermo Scientific	23225
Polypropylene Ultracentrifugation (UC) Tubes	Sorvall	03-141
Polystyrene Spheres 147 nm	Thermo Scientific	3150A
Polystyrene Spheres 125 nm	Thermo Scientific	3125A
Polystyrene Spheres 100 nm	Thermo Scientific	3100A
Polystyrene Spheres 70 nm	Thermo Scientific	3070A
Polystyrene Spheres 90 nm	Thermo Scientific	3090A
Protease Inhibitor Cocktail	Millipore Sigma	11697498001
RIPA	Cell Signaling Technology	9806
Roswell Park Memorial Institute (RPMI) 640 Medium	Gibco	11875093
Silica Nanosphere Cocktail	NanoFCM	n/a
SuperSignal West Pico PLUS Chemiluminescent Substrate	Thermo Scientific	34577
Swinging Bucket Rotor AH-629	Thermo Scientific	54284
Tris Buffered Saline (TBS)	Bio-Rad	1706435
Tween-20	Millipore Sigma	P7949
U937 Cell Line	American Type Culture Collection	CRL-1593.2
Ultra-Pure Distilled Water	Invitrogen	10977015
Uranyl Acetate	Polysciences	2144725

245
246
247
248

249   **RESULTS**

250

251   **Production, separation, and quality control of input materials**

252   Supernatants were collected from cultured human cell lines: H9 (T-lymphocytic) and U937 (pro-

253   monocytic). EVs were separated by size exclusion chromatography and ultrafiltration or

254   differential ultracentrifugation (Figure 1A). Marker expression and morphology were assessed

255   by WB (Figure 1B and Supplementary Figure 1) and TEM. WB revealed characteristic CD63

256   and CD81 expression patterns, with CD81 above the limit of detection only for H9 (Figure 1B).

257   Heterogeneous EV populations were observed by TEM in each sample preparation method

258   (Figure 1C). Additionally, we confirmed size and purity of silica spheres and polystyrene spheres

259   using TEM (Figure 1D).

260

261   **Artificial nanoparticle sizing**

262   Mixed silica spheres (SS) with nominal diameters of 68 nm, 91 nm, 113 nm, and 151 nm were

263   measured with the four platforms. Please note that since the SP-IRIS technology uses affinity to

264   capture particles, we dried particle mixtures onto the surface of the SP-IRIS chips before

265   imaging. SP-IRIS identified four distinct populations with diameter modes around 75 nm, 100

266   nm, 120 nm, and 150 nm (Figure 2A). NTA detected a broad population distribution with a mode

267   around 105 nm diameter (Figure 2B). MRPS resolved four distinct peaks for each individual

268   chip, but this distinction was masked somewhat by averaging all results (Figure 2C; see also

269   Supplementary Figure 2). NFCM resolved four populations with distinct peaks at diameters of

270   approximately 66 nm, 85 nm, 112 nm, and 154 nm (Figure 2D). Polystyrene spheres (PS) with

271   nominal diameters 70 nm, 90 nm, 122 nm, and 152 nm were mixed to a nominal concentration of

272   1×10^{12} particles/mL. SP-IRIS detected four distinct peaks around 80 nm, 110 nm, 140 nm, and

15

273   170 nm (Figure 2E). NTA returned a broad population distribution centered around 105 nm

274   (Figure 2F). MRPS identified distinct peaks at diameters 71 nm, 92 nm, 123 nm, and 150 nm

275   (Figure 2G). For PS, nano-flow showed four populations around 85 nm, 120 nm, 170 nm, and

276   225 nm in diameter, as well as a possible smaller population around 60 nm (Figure 2H).

277

278   **Artificial nanoparticle counting**

279   In addition to particle size, we also assessed counts. For SP-IRIS, a mean of around 3000 SS

280   particles were detected per printed antibody spot (Figure 3A), with no overall differences

281   between groups of antibody spots (*i.e.,* three spots per chip each of three tetraspanins and an

282   isotype control; note that no differences would be expected, since particles were dried onto the

283   chips). However, per-spot events overall ranged from <2000 SS particles per spot to >4500 SS

284   particles per spot (Figure 3A). SP-IRIS performed similarly for PS. There were no differences

285   between antibody groups, with a mean of around 1400 events/antibody spot (Figure 3B), but

286   events per spot ranged from <1000 PS particles/spot to 3000 PS particles/spot. Interestingly,

287   based on the nominal PS bead concentration and the surface area of the chips and spots, 10,000

288   particles per spot would be expected (Figure 3B, dotted line). Following SP-IRIS measurements,

289   chips were probed with three fluorescently labeled antibodies (anti-CD81, anti-CD63, and anti-

290   CD9) to assess background binding. Background binding was negligible for both SS and PS

291   (Supplementary Figure 3A and B, respectively). Some outliers were observed for CD9 (SS) or

292   CD63 (PS); however, none exceeded 1000 events. Particle concentrations were also measured by

293   NTA, MRPS, and NFCM. For SS (Figure 3C), MRPS estimated a concentration approximately

294   one log higher than NTA (5.1×10^{11} particles/mL *vs*. 5.4×10^{10} particles/mL, respectively), with

295   NFCM in the middle (1.7×10^{11} particles/mL). For PS, all three methods were in close agreement

16

296   (Figure 3D). Furthermore, the measured concentration was very close to the nominal PS

297   concentration of 1×10^{12} particles/mL (Figure 3D, dotted line).

298

299   **Biological particle sizing**

300   EV preparations from H9 and U937 cell supernatants enriched by ultrafiltration and SEC (SEC

301   EVs) or by differential ultracentrifugation (100K EVs) were next measured using each platform.

302   For H9-derived materials, SP-IRIS returned an almost identical size distribution profile for both

303   EV enrichment methods (Figure 4A). In contrast, NTA, MRPS, and NFCM measured more

304   particles at smaller diameters for the 100K EVs compared with the SEC EVs with roughly

305   similar particle size distributions (Figure 4B-D). However, substantial variation between

306   replicates might limit the conclusions that can be drawn from this observation. For U937-derived

307   materials, SP-IRIS and NTA (Figure 4E,F) detected more particles at smaller diameters from the

308   100K EVs compared with the SEC-EVs, again with roughly similar particle size distribution.

309   MRPS produced equivalent particle size distribution and particle number between the two

310   enrichment techniques (Figure 4G). In contrast, NFCM detected a higher particle count of

311   smaller particle diameters from the SEC EVs than the 100K EVs, with the particle size

312   distributions significantly different. Again, variability between replicates limits conclusions.

313   Overall, the results are broadly consistent with the reported power-law size distribution of EVs

314   [21,22] and the expectation that UC pellets may contain non-EV extracellular particles (EPs)

315   around the same size as EVs [1].

316

317   **Biological particle counting**

318 Particle counts were next assessed. As before, we present the SP-IRIS data separately because

319 this platform does not provide an overall count, but rather a number of events detected on chips

320 printed with antibodies (shown here: to CD81 and to CD63 plus an isotype control). Consistent

321 with protein assay results, SP-IRIS shows that more H9 particles were captured by anti-CD81

322 than by anti-CD63 (Figure 5A) and that U937 particles could be captured by CD63 capture

323 antibodies and not CD81 capture antibodies (Figure 5B). For the remaining three platforms,

324 which measure overall concentration, several trends were apparent (Figure 5C,D). First, for both

325 the H9 and the U937 source, and for both EV separation methods, data were consistent with the

326 results of SS counting in that NTA, NFCM, and MRPS measurements ordinally ranked from

327 lowest particles/mL to highest particles/mL. Secondly, MRPS and NFCM measured greater

328 particle concentrations for 100K EVs than for SEC EVs (corrected for processing and dilution),

329 although NTA results were similar. Finally, this is in contrast to results for the PS particles,

330 where the three techniques produced equivalent particle counts.

331

332 **Single particle phenotyping by fluorescence**

333 The SP-IRIS results represent a type of single-particle phenotyping since diameter is measured

334 for individual particles captured by antibodies and thus putatively positive for an antigen.

335 Captured particles can additionally be probed with fluorescently labeled antibodies. For chips

336 incubated with H9 EVs (Figure 6A,B), EVs captured by CD81 were generally positive for CD81

337 by fluorescence, and many also appeared to be CD63 positive. In contrast, CD63 capture spots

338 were largely devoid of fluorescence, as were (most) control capture spots. For chips incubated

339 with U937 EVs (Figure 6C,D), events on CD63 capture spots were also positive for CD63 by

340 fluorescence. CD81-linked fluorescence was at background levels for all spots. Note that

341 numbers of "positive" events are higher in fluorescence mode than with SP-IRIS (Figure 5A,B),

18

342   likely, as discussed later, because fluorescence detection is more sensitive than reflectance

343   imaging.

344   For the two remaining platforms with fluorescence capabilities, NTA and NFCM, results are

345   shown as percent of total particles (Figure 6E-H). Approximately 40% to 50% of detected

346   particles from H9 cells were positive for CD81 according to fluorescent NTA, while little to no

347   CD81 signal was detected for U937 materials, consistent with protein assay results. However, we

348   could not detect CD63-linked signal by fluorescent NTA for any sample. In contrast, NFCM

349   detected either CD81 or CD63 on a small percentage of particles. The percentages were similar

350   for the two tetraspanins for H9-derived particles. For U937 material, CD63-positive particles

351   were more abundant than CD81-positive particles. No major differences between the SEC and

352   100K separation methods were apparent according to these data (Figure 6E-H).

353

354

355 **DISCUSSION**

356

357 This study evaluated the abilities of four orthogonal technology platforms to size, count, and/or

358 phenotype biological EVs and synthetic nanoparticles. Three of the technologies—SP-IRIS,

359 NTA, and NFCM—are optical in nature and can perform some form of

360 phenotyping/fluorescence analysis, while the other, MRPS, is an electric sensing platform that

361 we did not attempt to apply to particle phenotyping. Although numerous comparisons of EV

362 characterization platforms have been published previously [15,23–26], this study includes

363 NFCM and MRPS and focuses in part on single-particle phenotyping.

364

365 ***Detected particles: size-range sensitivity and refractive index matter.*** Whereas NTA, MRPS,

366 and NFCM accurately and consistently measured the concentration of a known mixture of

367 polystyrene particles, estimates of the number of silica particles varied substantially. NTA

368 measured approximately 10-fold fewer SS particles than MRPS, while NFCM measured ~ 3-fold

369 fewer SS particles than MRPS. Since SS have a lower refractive index ($n_{SS} \sim 1.42$ [27]) than PS

370 ($n_{PS} \sim 1.59$ [28]), one might predict that a mixture of EVs, with an even lower refractive index

371 than silica [23,29], would have an even larger range of measurements. Indeed, for EV

372 preparations, average counts by NTA and MRPS varied by between one and two orders of

373 magnitude. These outcomes emphasize that each platform has an effective range of measurement

374 that may change with properties of particle populations, especially refractive index. Thus,

375 differences in output in part reflect different or overlapping particle populations that can be

376 detected by the specific technologies, as indeed reported previously for several of these

377 technologies [30]. That is, NTA and MRPS are similarly capable to detect a wide range of PS

378 particle sizes. However, NTA may detect a more limited range of biological particles [31] than

20

379   the MRPS platform using a small pore-size cartridge, in that MRPS may detect more of the

380   smaller EVs along the power-law distribution. Signal for NTA scales with radius to the 6th

381   power, whereas signal scales for MRPS with radius to the 3rd power; thus, because of finite

382   dynamic range, NTA will be biased to detecting fewer of the small particles in a sample

383   compared with MRPS.

384

385   ***Is it important to resolve different particle size populations?*** SP-IRIS, MRPS, and NFCM could

386   resolve up to four populations of synthetic nanoparticles with different diameters. We note that

387   distinct populations were somewhat obscured when MRPS results were averaged for SS, but not

388   for PS – see Supplementary Figure 4 – which may reflect aggregation of the SS due to the

389   electrolyte solution (PBS) required for MRPS and the convolution of experimental uncertainties

390   in particle concentration and size measurements. Also noteworthy is that the NFCM platform

391   distinguished subpopulations of SS particles, but that this is likely because the same beads are

392   used to calibrate the instrument. While detecting the expected concentration of high refractive

393   index PS particles, NTA was unable to resolve individual particle populations and instead

394   characterized the SS particles as a broad population distribution centered on an "average" size.

395   To be sure, it may be possible to resolve discretely sized particle populations using NTA with

396   mixtures at different ratios of sizes. We could not do so with the mixtures we used. Whether this

397   matters for biological particles is unclear. It does not seem that biological samples would contain

398   unique EV subpopulations with exquisitely defined sizes, except perhaps for samples from

399   sources infected with specific enveloped viruses. NTA does seem to be capable of detecting

400   shifts in population distributions, and this capability might be more important for biological

401   particles than resolving subpopulations.

bioRxiv preprint doi: https://doi.org/10.1101/2020.08.04.237156; this version posted August 5, 2020. The copyright holder for this preprint (which was not certified by peer review) is the author/funder, who has granted bioRxiv a license to display the preprint in perpetuity. It is made available under aCC-BY 4.0 International license.

402

403   ***On counting by SP-IRIS/fluorescence.*** One clear finding of our study is that, in our hands,

404   neither SP-IRIS label-free measurements nor subsequent fluorescence detection could be used

405   directly to estimate overall particle concentration. Instead, SP-IRIS is best used to understand

406   ratios within populations and for single-particle phenotyping. Even when PS beads were dried

407   onto chips, the measured concentration was approximately one-seventh of the expected

408   concentration. While uneven drying could contribute, it seems that PS particles non-specifically

409   adhered to the chip without a washing step, were undercounted slightly. For biological particles,

410   the problem is compounded since only a subset of EVs bind to any given affinity reagent "spot."

411   Binding is determined by diffusion (which is slow for EVs), presence and density of recognized

412   surface markers, and affinity characteristics of antibody-to-antigen binding. The bound

413   population of particles remaining after wash steps is only a miniscule proportion of the total in

414   the input material and cannot be used to determine overall concentration. Interestingly,

415   fluorescence results often indicated higher particle concentrations than returned by label-free

416   counting, even though particles positive for a particular antigen are expected to be only a subset

417   of the captured population (different antigens) or to approach equality (if the capture antigen is

418   targeted and antigen is abundant). Counts are higher because fluorescence detection is more

419   sensitive than label-free. That is, fluorescence detects positive particles that may be below the

420   limit of label-free detection.

421

422   ***Did any platforms identify differences between EV separation technologies?*** For both

423   biological sources of EVs, we used two methods of EV separation: dUC (100K EVs), which has

424   been the most common method for EV separation [32,33], and a combination of filtration and

22

425   size exclusion chromatography (SEC EVs) [34,35]. According to some evidence in the literature,

426   dUC leads to more protein contamination and aggregation and damage of EVs [36–38]. It should

427   be noted that alternative viewpoints can also be found [16]. However, protein particle

428   contamination might be expected to introduce more and smaller particles. This outcome is indeed

429   observed based upon TEM background and particle profile shifts towards smaller particles for

430   several of the platforms. For SP-IRIS with fluorescence, it is also interesting that tetraspanin

431   positivity is higher for samples obtained by SEC than with dUC. On the other hand, evidence of

432   aggregation by dUC is not apparent in the data presented here. We cannot rule out aggregation,

433   however, only that the techniques used here did not appear to detect it.

434

435   ***Single-particle phenotyping.*** For the three techniques with single-particle phenotyping

436   capabilities (SP-IRIS, NTA, and NFCM), each has advantages and drawbacks, as covered above,

437   all can potentially provide true single-particle phenotyping data. SP-IRIS was able to achieve the

438   most "multiplexed" detection, in that signal could be obtained above background for up to three

439   fluorescent channels. At the time of our evaluations, the NTA platform we used could not

440   perform simultaneous multi-channel measurements and thus was not a true single-particle

441   multiplexing platform. Instead, sequential filter switches were required, such that the same

442   particles could not be tracked in different channels.

443

444   In Table 2, we attempt to summarize our findings and views about the four investigated

445   techniques. **Detectable size ranges** for biological particles: these should be considered to be

446   rough estimates. If we accept the assumption that EVs follow a power-law size distribution (the

447   smaller, the more abundant, with lower bounds defined by membrane curvature constraints), then

23

448   no evaluated platform effectively detects the very smallest particles. However, SP-IRIS, MRPS,

449   and NFCM appear to detect slightly smaller particles than NTA under the conditions and settings

450   we tested. For NTA, MRPS, and NFCM, linear ranges for **particle concentration** for all

451   instruments begin around 1×10^7 particles/mL and extend from about one order of magnitude

452   (NTA) to multiple orders of magnitude (MRPS). This spread is important, since the wider the

453   range, the fewer time-consuming concentrations or dilutions must be done to place an unknown

454   particle population into the measurable range. SP-IRIS is a special case, since particles are

455   captured by affinity, and overall concentration cannot easily be estimated. In our hands, particle

456   concentrations must be high ($>>1 \times 10^7$ particles /mL) even for abundant antigens. Furthermore,

457   the optimal captured particle counts are roughly 3000 to 6000 per antibody spot (although this

458   may vary). To hit a very tight "sweet spot", many trial dilutions may be needed. Furthermore, the

459   optimal dilution may well be different for different antibodies on the chip because of different

460   percentages of EVs positive for a particular antigen, per-EV antigen abundance, and antibody

461   performance. Hence, dilutions are usually most important and time-consuming for SP-IRIS.

462   Related to dilution is the **volume of input material** required for a single reading. Assuming each

463   platform can measure 1×10^7 particles per mL, the required volume of a dilution at this

464   concentration ranges from 5 ul (MRPS) to around 1 mL (NTA). Of course, the actual

465   volume/number of EVs needed will also depend on the number of concentrations/dilutions

466   required to reach the measurable concentration range. The input volume difference is also

467   inconsequential for highly abundant materials, but may be important for low-abundance EV

468   samples. **If done, optional calibration steps** are rapid for NTA and MRPS (around 20 minutes).

469   For NFCM, we find that calibration can be as short as 20 minutes but can sometimes take longer.

470   Time for sample dilutions is most difficult to estimate, but is expected to correlate inversely with

24

471   the range of measurement for each platform. **Read time** ranges from five minute to about half an

472   hour per sample. Note that the times we indicate are for sizing and counting only. Optional

473   fluorescence measurements for the relevant platforms would in some cases add processing time

474   for antibody incubations and removal, as well as for read times (except for NFCM). For SP-IRIS,

475   we should also note that, although the total hands-on and read time is longer than for other

476   techniques, each reading includes on-chip replicates, multiple capture antibodies, and up to three

477   fluorescence readouts per capture antibody.

478

479   **Costs** for the platforms include initial outlay, disposable costs, and maintenance costs. For

480   acquisition, the MRPS system is most economical, while NFCM is the most expensive. For basic

481   counting and sizing, operating costs for NTA and NFCM are negligible. Adding optional

482   fluorescence increases these costs by amounts that are antibody-dependent. The MRPS system

483   uses disposable cartridges that currently cost USD 8 to USD 12 each. The SP-IRIS platform has

484   the highest disposable costs, with each sample requiring at least one chip at USD 50 to >USD

485   100 each. Since optimal dilutions are difficult to achieve and may be different for different

486   capture materials on the same chip, multiple chips may be needed for the same sample. Chips

487   also cannot be chemically stripped and re-used, at least not in our hands (Mallick and Witwer,

488   unpublished data). Furthermore, we find that chips often go unused and are thus "wasted" as a

489   result of a short shelf life of only several weeks. Since chips may take several weeks (or more for

490   custom) to procure, the three-week shelf life requires excellent planning and a lack of

491   unexpected difficulties in the laboratory; otherwise, the investment is wasted. As noted, though,

492   under optimal conditions, the platform provides multi-dimensional information that may justify

493   these costs and logistical challenges for some users. We should also mention that chips for the

494   SP-IRIS and MRPS instruments are currently available only from the instrument manufacturer

495   for that particular measurement technique. As for maintenance costs, we are unable to estimate

496   them at this time.

497

498   **In conclusion:**

499   • No evaluated platform is necessarily "better" or "worse" than others; rather, it is

500   important to be aware of the capabilities of each platform with respect to each particle

501   population of interest.

502   • Rather than relying on a single platform, consider using orthogonal technologies.

503   • Both acquisition and recurring costs should be considered before acquiring a platform.

504   Appropriate reference materials are needed for better evaluation of single particle phenotyping

505   capabilities, including multiplexed phenotyping.

506

507

508

509　**FIGURE LEGENDS**

510

511　**Figure 1: Methodology and EV separation.** (A) EVs were isolated from H9 and U937

512　conditioned cell media by a combination of ultrafiltration and size exclusion chromatography

513　(SEC EVs) or by differential ultracentrifugation (100K EVs). (B) Immunoblot analysis of

514　isolated EVs as well as corresponding cell lysates from H9 and U937 using antibodies specified

515　in Table 1; see also Supplementary Figure 1. (C) Electron microscopy images of SEC EV and

516　100K EV samples from both cell lines. Leftmost scale bars 500 nm and magnification 40 000×;

517　rightmost scale bars 100 nm and magnification 100 000×. (D) EM of SS and PS. Leftmost scale

518　bars 500 nm and magnification 17 500×; rightmost scale bars 100 nm and magnification 65

519　000×.

520

521　**Figure 2: SS and PS size distribution.** Size distributions for SS (n=3) with standard deviation

522　for (A) SP-IRIS, (B) NTA, (C) MRPS, and (D) NFCM. Nominal SS diameters are at the vertical

523　dotted lines: 68 nm, 91 nm, 113 nm, and 151 nm. Size distributions for PS (n=3; with SD) for (E)

524　SP-IRIS, (F) NTA, (G) MRPS, and (H) NFCM. Nominal PS diameters are at the vertical dotted

525　lines: 70 nm, 90 nm, 122 nm, and 152 nm. Insert in Figure 2C shows a single MRPS

526　measurement of the size distribution.

527

528　**Figure 3: SS and PS quantification.** (A) SP-IRIS label-free capture for SS and PS using four

529　capture spots (n=3 per group; mean particle count per spot with SD). B) SS quantification (n=3;

530　mean particles/mL with SD). (C) PS quantification (n=3; mean particles/mL with SD). Nominal

531　PS concentration is portrayed with a horizontal line (1.0×10^{12} particles/mL).

532

Figure 4: H9 and U937 particle size distribution. Diameters of particles for H9 SEC EVs and 100K EVs (n=3 per group, with standard deviation) for (A) SP-IRIS, (B) NTA, (C) MRPS, and (D) NFCM. Size distributions for U937 SEC EVs and 100K EVs (n=3 per group; with SD) for (E) SP-IRIS, (F) NTA, (G) MRPS, and (H) NFCM.

537

Figure 5: H9 and U937 particle quantification. SP-IRIS label-free capture for (A) H9 SEC EVs and 100K EVs and (B) U937 SEC EVs and 100K EVs using CD81, CD63, and mouse isotype control capture antibodies (n=3 per group; mean particle count/spot with SD). H9 and U937 particle quantification (n=3; mean particles/mL with SD) for (C) SEC EVs and (D) 100K EVs using NTA, MRPS, and NFCM.

543

Figure 6: Particle phenotyping. SP-IRIS fluorescence detection using labeled anti-CD81 and anti-CD63 after particle capture with CD81, CD63, and mouse isotype control (n=3 per group; mean and SD) for (A) H9 SEC EVs, (B) H9 100K EVs, (C) U937 SEC EVs, and (D) U937 100K EVs. Percent of particles detected with fluorescently-labeled anti-CD81 and anti-CD63 by NTA and NFCM (n=3 per group; mean and SD) for (E) H9 SEC EVs, (F) H9 100K EVs, (G) U937 SEC EVs, and (H) U937 100K EVs. Asterisk. An asterisk indicates that, in the authors' view, an antibody did not perform on the instrument; it does not necessarily mean that the antibody would not perform in another context or with additional optimization.

552

28

553   **Supplementary Figure 1: Additional EV characterization.** (A) BCA assay results, including

554   final protein concentrations in µg/mL. (B) Immunoblot analysis of separated EVs as well

555   as corresponding cell lysates from H9 and U937 using antibodies specified in Table 1.

556

557   **Supplementary Figure 2: Individual SS measurements by MRPS.** Repeats 2 (A) and 3 (B)

558   for SS using MRPS. Repeat 1 can also be found as an inset in Figure 2C.

559

560   **Supplementary Figure 3: SP-IRIS background fluorescence for SS and PS.** SP-IRIS

561   fluorescence detection using fluorescently labeled anti-CD81, anti-CD63, and anti-CD9 after (A)

562   SS and (B) PS capture with four antibody groups (n=3 per group; mean and SD).

563

564   **Supplementary Figure 4: MRPS and NFCM dilution series.** SS (A) and PS (B) were diluted

565   2×, 5×, and 10× by volume to determine the optimal dilution for NTA analysis. SS (C) were

566   diluted 1:1000 (v:v), 1:2000 (v:v), and 1:4000 (v:v) and PS (D) were diluted 1:2500 (v:v),

567   1:5000 (v:v), and 1:10000 (v:v) to determine the optimal dilution for NFCM analysis. Dilution-

568   corrected counts are for SS (E) and PS (F) on MRPS and SS (G) and PS (H) on NFCM. Optimal

569   dilutions are indicated by green or yellow (MRPS and NFCM, respectively).

570

571   **Supplementary Table 1: Antibodies tested with fluorescent NTA.** H9 100K EVs were diluted

572   1:1 (v:v) in PBS. 9 µL of diluted EVs were mixed with 1 µL of antibody and incubated for 2

573   hours at room temperature. Samples were then diluted 1:1000 and measured in scatter and

574   fluorescent modes using NTA.

575

576
577

578   **Acknowledgements:**

579   The authors thank members of the Witwer and Retrovirus Laboratories and various members of

580   the International Society for Extracellular Vesicles for discussions and support. The Authors

581   acknowledge NanoView Biosciences, Particle Metrix, Spectradyne, and NanoFCM

582   representatives for discussions and for arranging demonstrations. Electron microscopy images

583   were acquired in the Johns Hopkins University School of Medicine Institute for Basic

584   Biomedical Sciences Microscope Facility.

585

586   **Disclosure Statement:**

587   Authors report no conflicts of interest.

588

589   **Funding:**

595

REFERENCES

[1] Théry C, Witwer KW, Aikawa E, et al. Minimal information for studies of extracellular vesicles 2018 (MISEV2018): a position statement of the International Society for Extracellular Vesicles and update of the MISEV2014 guidelines. J Extracell Vesicles 2018;7:1535750.

[2] Yáñez-Mó M, Siljander PR-M, Andreu Z, et al. Biological properties of extracellular vesicles and their physiological functions. J Extracell Vesicles 2015;4:27066.

[3] Witwer KW, Théry C. Extracellular vesicles or exosomes? On primacy, precision, and popularity influencing a choice of nomenclature. J Extracell Vesicles 2019;8:1648167.

[4] Cocucci E, Meldolesi J. Ectosomes and exosomes: shedding the confusion between extracellular vesicles. Trends Cell Biol 2015;25:364–72.

[5] Lázaro-Ibáñez E, Lässer C, Shelke GV, et al. DNA analysis of low- and high-density fractions defines heterogeneous subpopulations of small extracellular vesicles based on their DNA cargo and topology. Https://DoiOrg/101080/2001307820191656993 2019.

[6] Russell AE, Sneider A, Witwer KW, et al. Biological membranes in EV biogenesis, stability, uptake, and cargo transfer: an ISEV position paper arising from the ISEV membranes and EVs workshop. J. Extracell. Vesicles, vol. 8, Taylor and Francis Ltd.; 2019.

[7] Tkach M, Kowal J, Théry C. Why the need and how to approach the functional diversity of extracellular vesicles. Philos Trans R Soc Lond B Biol Sci 2018;373:20160479.

[8] Lässer C, Jang SC, Lötvall J. Subpopulations of extracellular vesicles and their therapeutic potential. Mol Aspects Med 2018;60:1–14.

[9] Lanier LL, Engleman EG, Gatenby P, et al. Correlation of functional properties of human lymphoid cell subsets and surface marker phenotypes using multiparameter analysis and flow cytometry. Immunol Rev 1983;74:143–60.

[10] Reddington AP, Trueb JT, Freedman DS, et al. An Interferometric Reflectance Imaging Sensor for Point of Care Viral Diagnostics. IEEE Trans Biomed Eng 2013;60:3276–83.

[11] Lopez CA, Daaboul GG, Vedula RS, et al. Label-free multiplexed virus detection using spectral reflectance imaging. Biosens Bioelectron 2011;26:3432–7.

[12] Dragovic RA, Gardiner C, Brooks AS, et al. Sizing and phenotyping of cellular vesicles using Nanoparticle Tracking Analysis. Nanomedicine 2011;7:780–8.

[13] Sokolova V, Ludwig AK, Hornung S, et al. Characterisation of exosomes derived from human cells by nanoparticle tracking analysis and scanning electron microscopy. Colloids Surf B Biointerfaces 2011;87:146–50.

[14] Giebel B, Helmbrecht C. Methods to analyze EVs. Methods Mol. Biol., vol. 1545, Humana Press Inc.; 2017, p. 1–20.

[15] Anderson W, Kozak D, Coleman VA, et al. A comparative study of submicron particle sizing platforms: Accuracy, precision and resolution analysis of polydisperse particle size distributions. J Colloid Interface Sci 2013;405:322–30.

[16] Tian Y, Gong M, Hu Y, et al. Quality and efficiency assessment of six extracellular vesicle isolation methods by nano-flow cytometry. J Extracell Vesicles 2020;9.

[17] Tian Y, Ma L, Gong M, et al. Protein Profiling and Sizing of Extracellular Vesicles from Colorectal Cancer Patients via Flow Cytometry. ACS Nano 2018;12:671–80.

[18] Ahn JY, Datta S, Bandeira E, et al. Release of extracellular vesicle miR-494-3p by ARPE-19 cells with impaired mitochondria. Biochim Biophys Acta Gen Subj 2020:129598.

642 [19] Gámbaro F, Li Calzi M, Fagúndez P, et al. Stable tRNA halves can be sorted into
643 extracellular vesicles and delivered to recipient cells in a concentration-dependent manner.
644 RNA Biol 2019.

645 [20] Huang Y, Cheng L, Turchinovich A, et al. Influence of species and processing parameters
646 on recovery and content of brain tissue-derived extracellular vesicles. J Extracell Vesicles
647 2020;9:1785746.

648 [21] van der Pol E, Böing AN, Gool EL, et al. Recent developments in the nomenclature,
649 presence, isolation, detection and clinical impact of extracellular vesicles. J Thromb
650 Haemost 2016;14:48–56.

651 [22] Paulaitis M, Agarwal K, Nana-Sinkam P. Dynamic Scaling of Exosome Sizes. Langmuir
652 2018;34:9387–93.

653 [23] Van Der Pol E, Coumans FAW, Sturk A, et al. Refractive index determination of
654 nanoparticles in suspension using nanoparticle tracking analysis. Nano Lett
655 2014;14:6195–201.

656 [24] Bachurski D, Schuldner M, Nguyen PH, et al. Extracellular vesicle measurements with
657 nanoparticle tracking analysis–An accuracy and repeatability comparison between
658 NanoSight NS300 and ZetaView. J Extracell Vesicles 2019;8.

659 [25] Erdbrügger U, Lannigan J. Analytical challenges of extracellular vesicle detection: A
660 comparison of different techniques. Cytom Part A 2016;89:123–34.

661 [26] Corso G, Heusermann W, Trojer D, et al. Systematic characterization of extracellular
662 vesicles sorting domains and quantification at the single molecule–single vesicle level by
663 fluorescence correlation spectroscopy and single particle imaging. J Extracell Vesicles
664 2019;8.

665 [27] García-Santamaría F, Míguez H, Ibisate M, et al. Refractive index properties of calcined
666 silica submicrometer spheres. Langmuir 2002;18:1942–4.

667 [28] Kasarova SN, Sultanova NG, Ivanov CD, et al. Analysis of the dispersion of optical
668 plastic materials. Opt Mater (Amst) 2007;29:1481–90.

669 [29] Gardiner C, Shaw M, Hole P, et al. Measurement of refractive index by nanoparticle
670 tracking analysis reveals heterogeneity in extracellular vesicles. J Extracell Vesicles
671 2014;3.

672 [30] van der Pol E, Coumans FAW, Grootemaat AE, et al. Particle size distribution of
673 exosomes and microvesicles determined by transmission electron microscopy, flow
674 cytometry, nanoparticle tracking analysis, and resistive pulse sensing. J Thromb Haemost
675 2014;12:1182–92.

676 [31] Defante AP, Vreeland WN, Benkstein KD, et al. Using Image Attributes to Assure
677 Accurate Particle Size and Count Using Nanoparticle Tracking Analysis. J Pharm Sci
678 2018;107:1383–91.

679 [32] Théry C, Amigorena S, Raposo G, et al. Isolation and Characterization of Exosomes from
680 Cell Culture Supernatants and Biological Fluids. Curr. Protoc. Cell Biol., vol. Chapter 3,
681 Hoboken, NJ, USA: John Wiley & Sons, Inc.; 2006, p. Unit 3.22.

682 [33] Gardiner C, Di Vizio D, Sahoo S, et al. Techniques used for the isolation and
683 characterization of extracellular vesicles: results of a worldwide survey. J Extracell
684 Vesicles 2016;5:32945.

685 [34] Böing AN, van der Pol E, Grootemaat AE, et al. Single-step isolation of extracellular
686 vesicles by size-exclusion chromatography. J Extracell Vesicles 2014;3:23430.

687 [35] Théry C, Witwer KW, Aikawa E, et al. Minimal information for studies of extracellular

33

688   vesicles 2018 (MISEV2018): a position statement of the International Society for
689   Extracellular Vesicles and update of the MISEV2014 guidelines. J Extracell Vesicles
690   2019;8:1535750.
691   [36] Linares R, Tan S, Gounou C, et al. High-speed centrifugation induces aggregation of
692   extracellular vesicles. J Extracell Vesicles 2015;4:29509.
693   [37] Van Deun J, Mestdagh P, Sormunen R, et al. The impact of disparate isolation methods
694   for extracellular vesicles on downstream RNA profiling. J Extracell Vesicles
695   2014;3:24858.
696   [38] Arab T, Raffo-Romero A, Van Camp C, et al. Proteomic characterisation of leech
697   microglia extracellular vesicles (EVs): comparison between differential ultracentrifugation
698   and Optiprep^{TM} density gradient isolation. J Extracell Vesicles 2019;8:1603048.
699

Figure 1. Methodology and EV separation
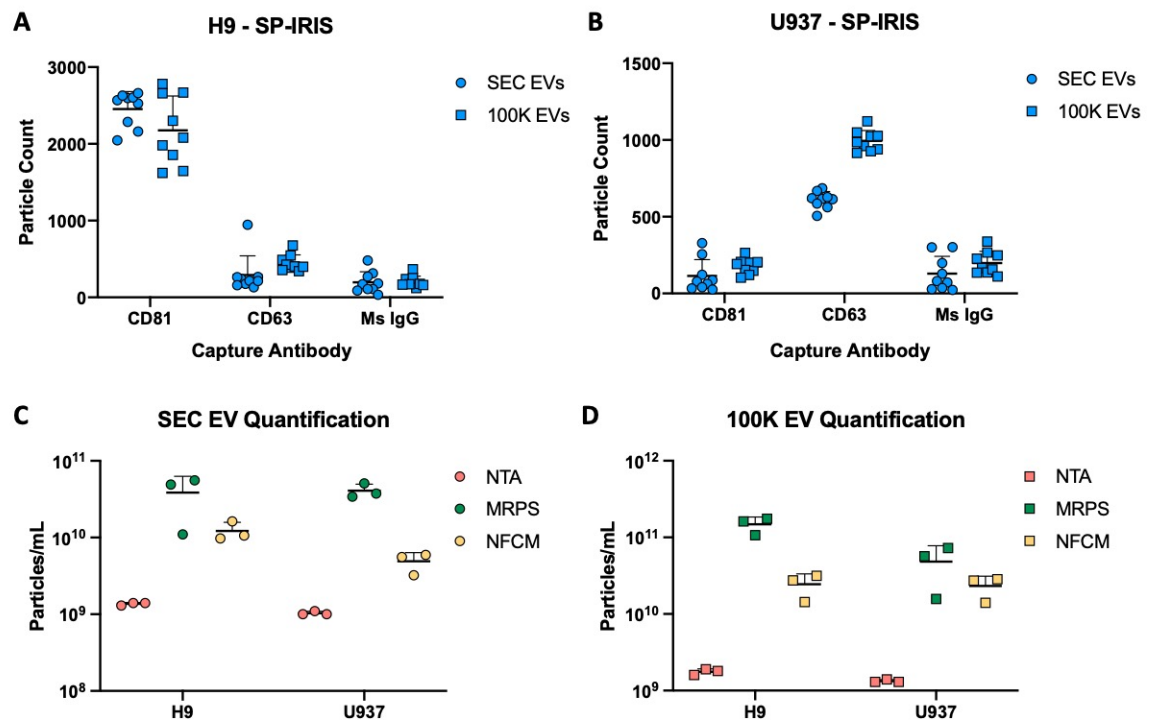

700
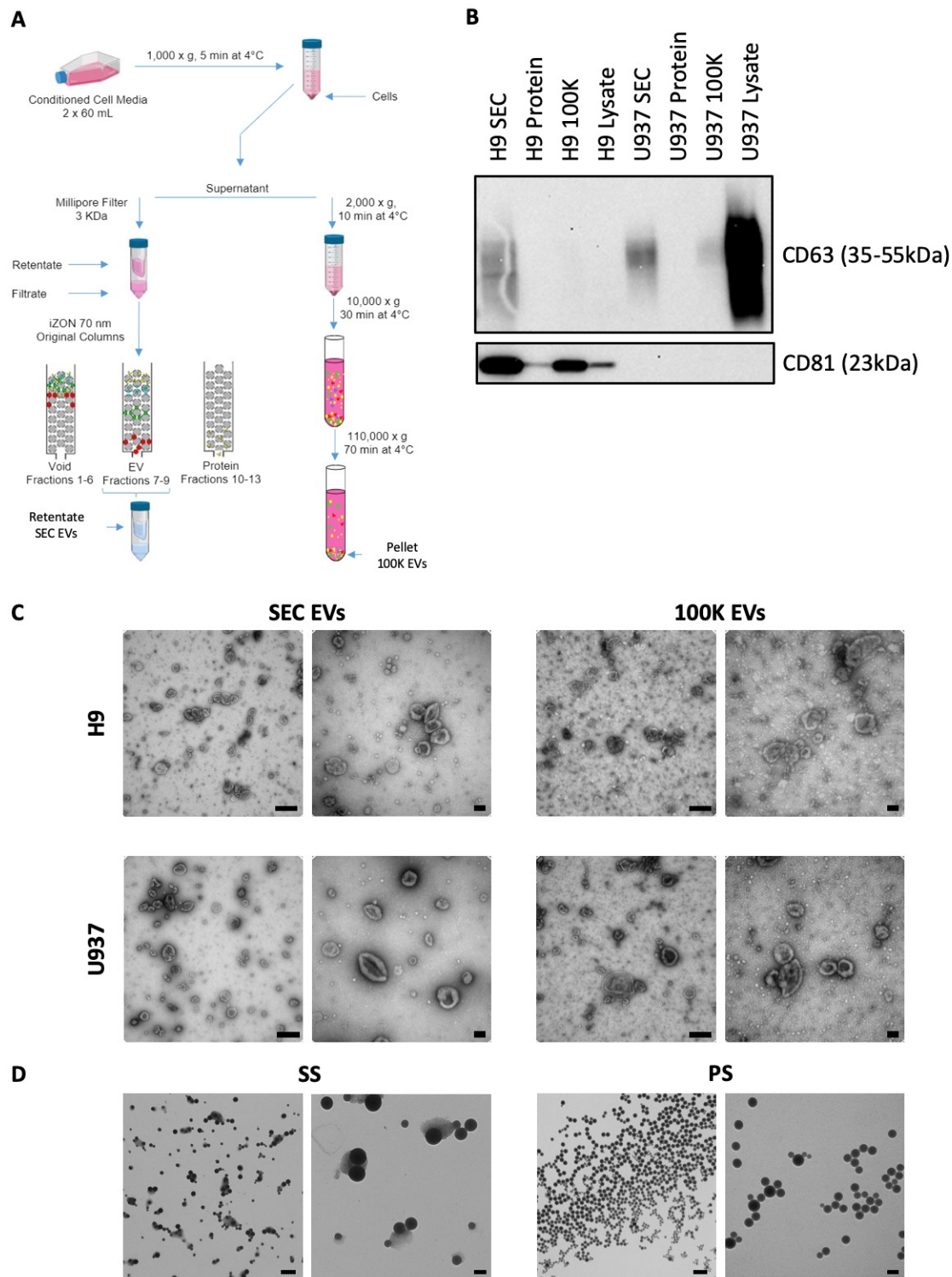
Figure 2. SS and PS size distribution
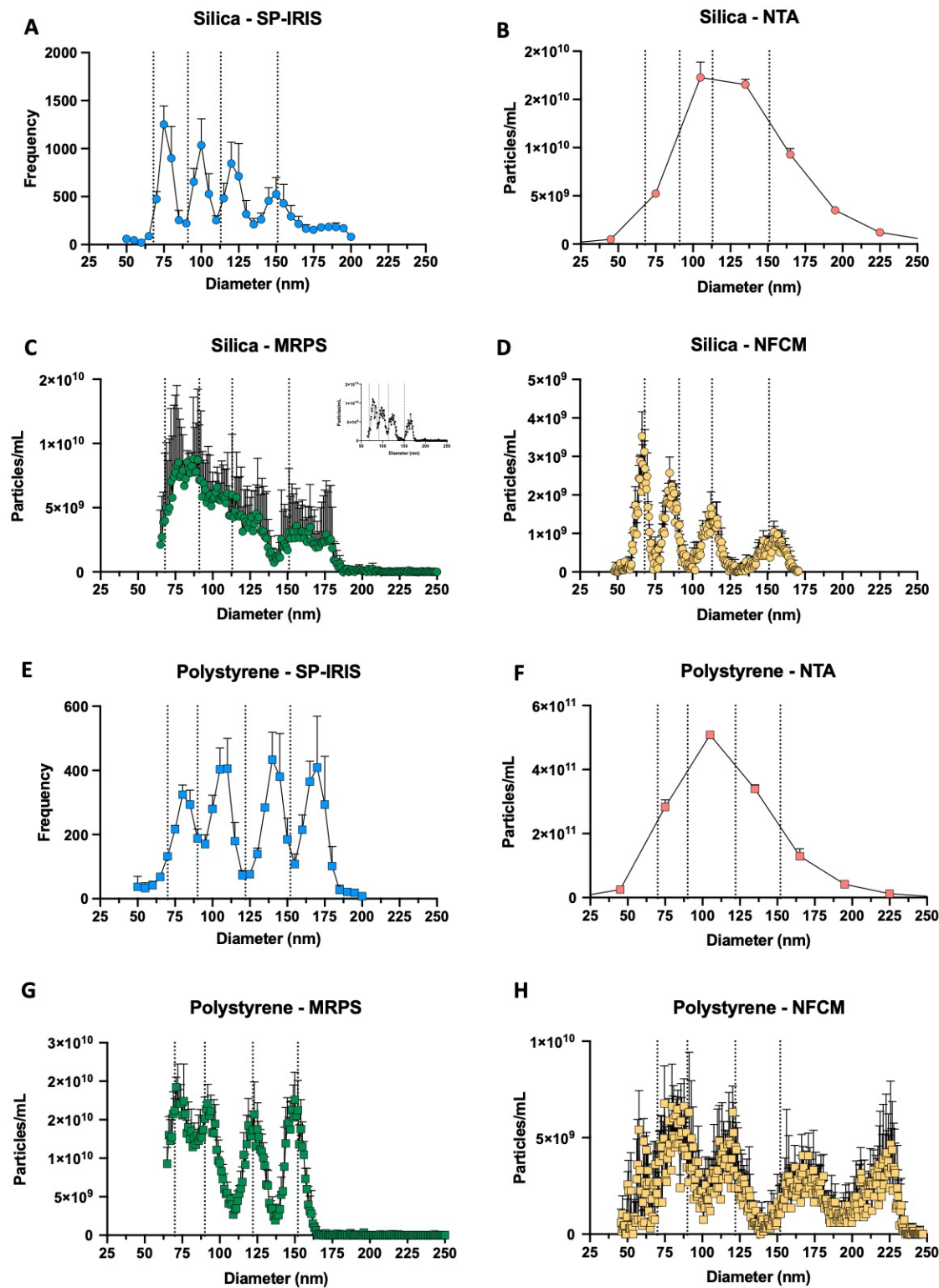
Figure 3. SS and PS quantification
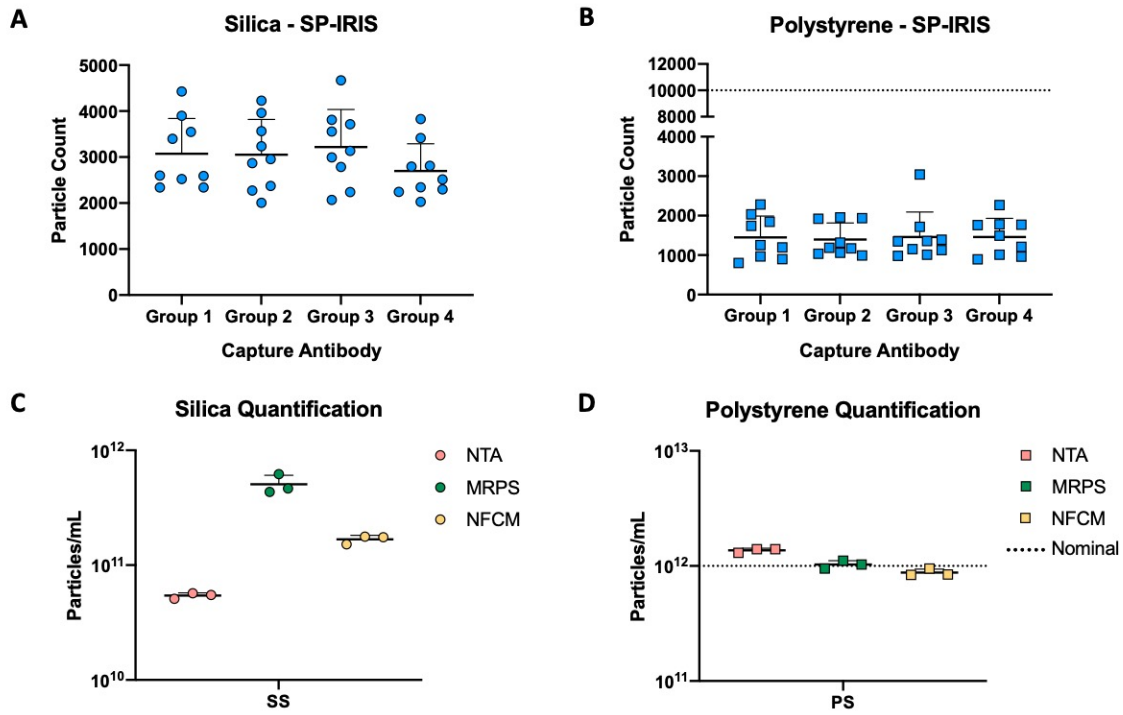
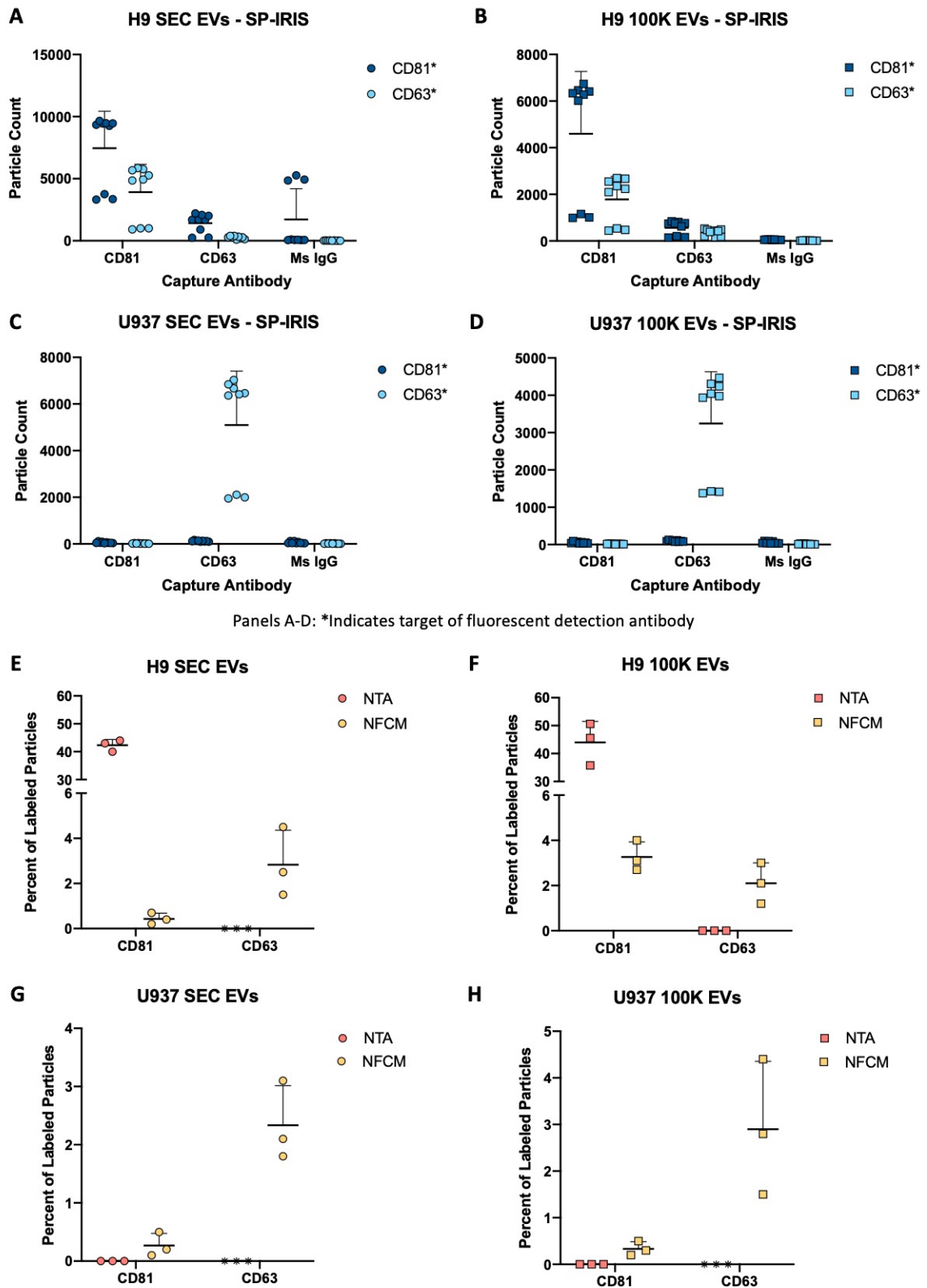## Figure 4. H9 and U937 Size Distribution
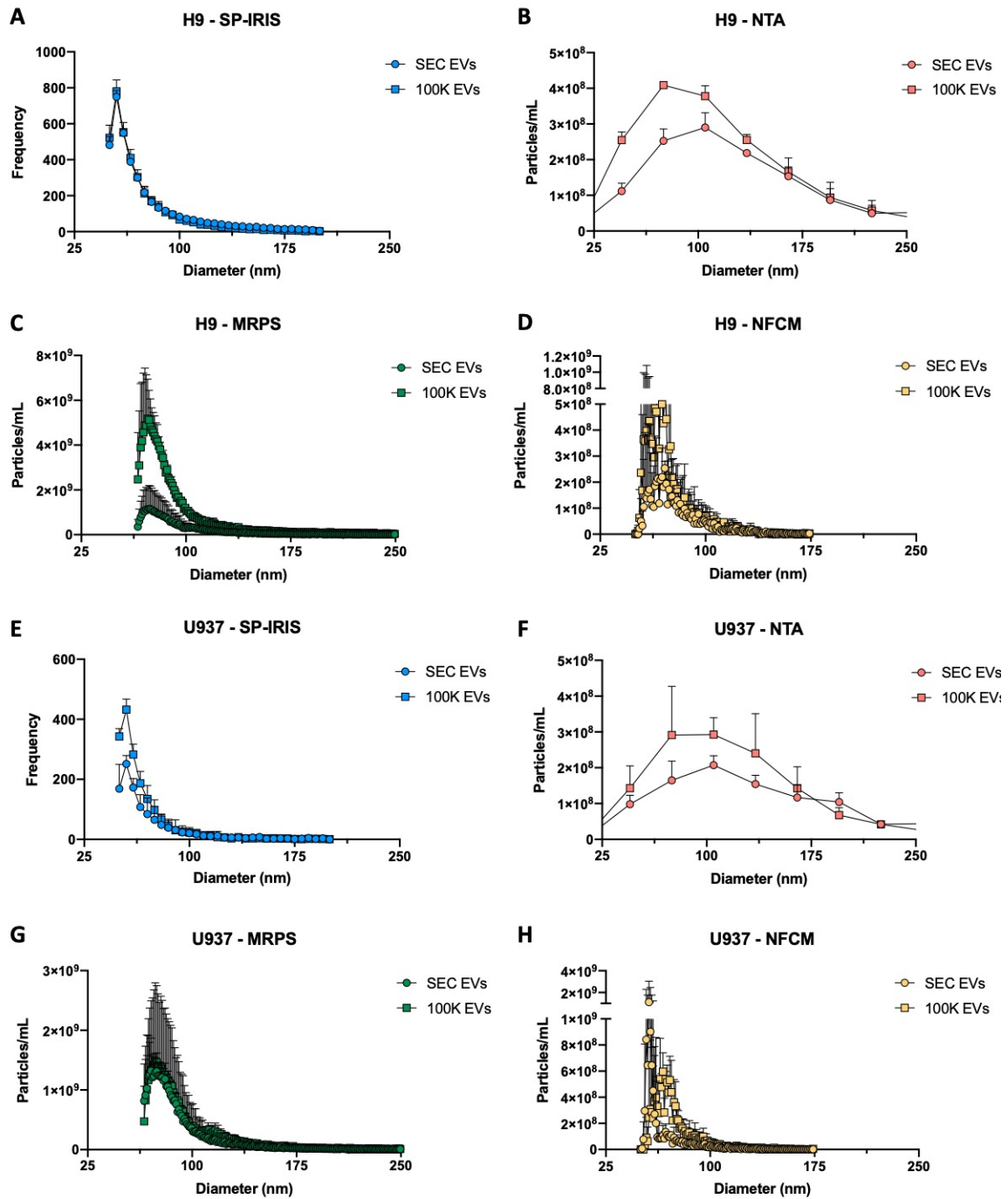
Figure 5. H9 and U937 particle quantification

Figure 6. Particle phenotyping

Panels A-D: *Indicates target of fluorescent detection antibody

Table 2. Evaluation summary

Technique	Logistics						Performance		
	Estimated biological particle size detection range (diameter)	Concentration Detection Range	Input volume (µl; may be a dilution)	Operation Time: Hands-on (HO)/ Read time (R) (does not include optional labeling)	Instrument Cost	Costs for disposables	Sizing (including discrimination of different size populations)	Quantification (across all particles, biological and synthetic)	Fluorescence (channels; for instruments we evaluated)
SP-IRIS	~50 nm to 200 nm	n/a; depends on capture Ab, but >>1×10^7 particle/mL preferred	35	Day 1: 10 min sample prep (HO) Day 2: 2 hour (HO); 10 min to 30 min per sample (R)	$$	$$$: Chip/antibody kits (starting at $50/sample to >$100 for custom; ordered from manufacturer)	++	-	Up to 3
NTA	~70 nm to several hundred nm	1×10^7 to 1×10^8 particle/mL (in PBS)	1000	Optional 20 min calibration (HO/P); 5 min to 15 min per sample (HO/R)	$$	$: <$1 per sample: 1 mL syringes ($23 per 100, multiple suppliers; Ab not included)	+	+	Up to 4
MRPS	~50 nm to 2 µm (cartridge-dependent)	1×10^7 to 1×10^{10} particle /mL (in PBS/PBST)	5	Optional 20 min calibration (HO/R); 15 min to 30 min per sample (HO/R)	$	$$: Cartridges ($8 to $12 each, ordered from manufacturer)	++	++	n/a
NFCM	~40 nm to 170 nm	1×10^7 to 1×10^9 particle/mL (in PBS)	20	20 min to 120 min calibration (HO/P); 5 min per sample (HO/P)	$$$	$: <$1 per sample: 0.5 mL Tubes ($27 per 1000, multiple suppliers; Ab not included)	++	++	Up to 2

RI = refractive index; p/mL = particles per milliliter; Price range: $$$ > $$ > $; values in USD;
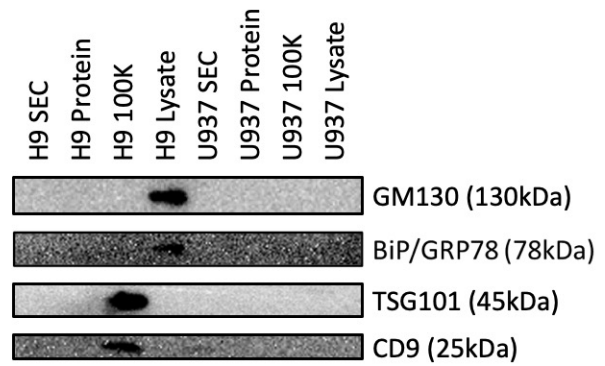Performance indicator: +++ > ++ > + > -

706

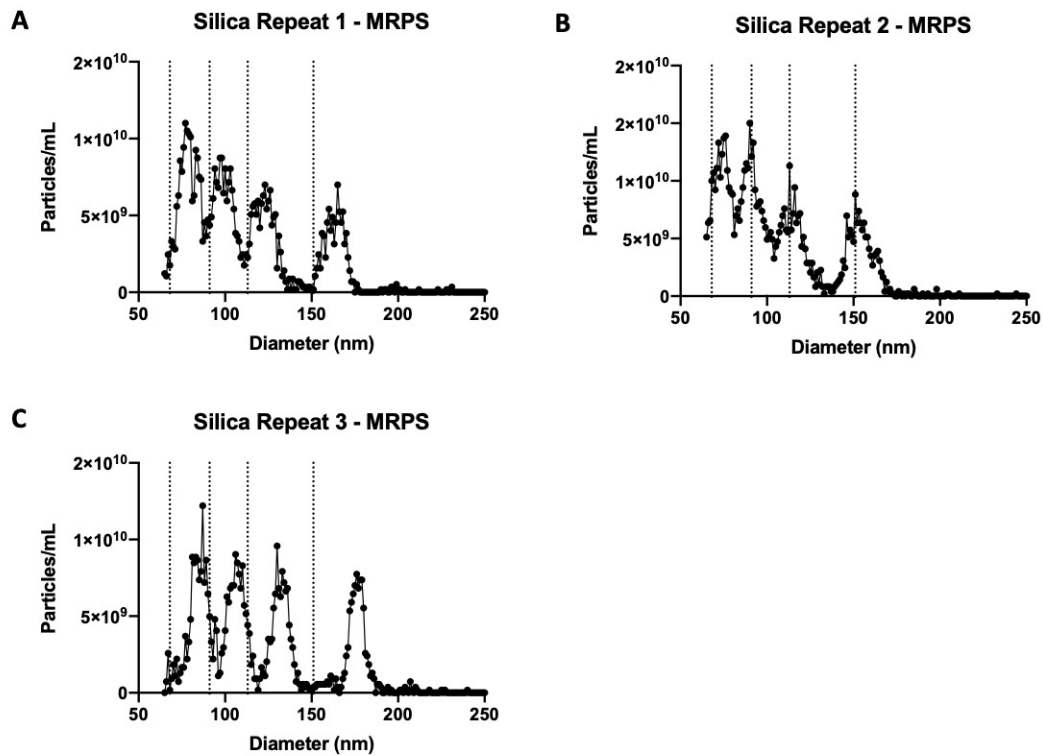## Supplementary Figure 1. Additional EV characterization

A
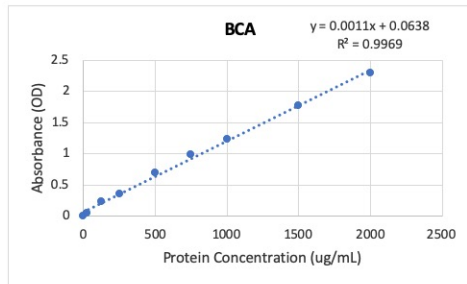
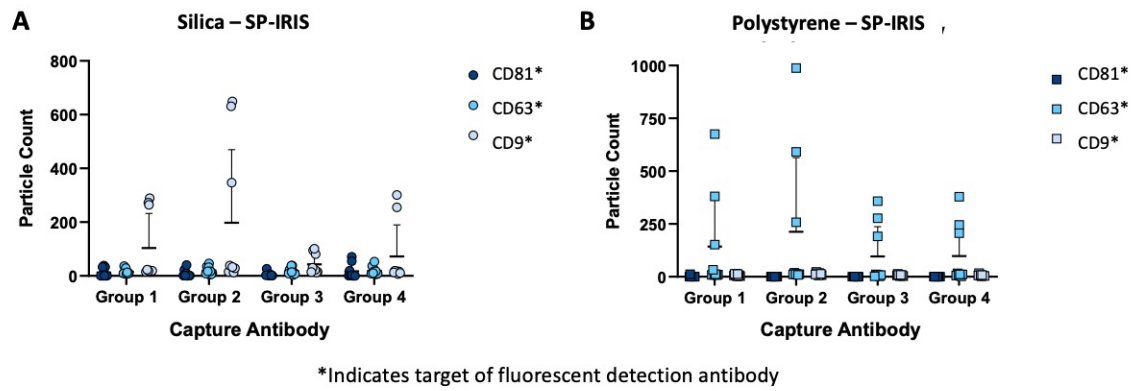| Sample	Protein Concentration (ug/mL)
H9 SEC	762.42
H9 Protein	1547.27
H9 100K	2013.94
H9 Cell lysate	3941.21
U937 SEC	550.30
U937 Protein	1762.42
U937 100K	1747.27
U937 Cell lysate	6320.00

B

707

Supplementary Figure 2. Individual SS measurements by MRPS

708

Supplementary Figure 3. SP-IRIS background fluorescence for SS and PS

*Indicates target of fluorescent detection antibody

709

Supplementary Figure 4. MRPS and NFCM dilution series

710
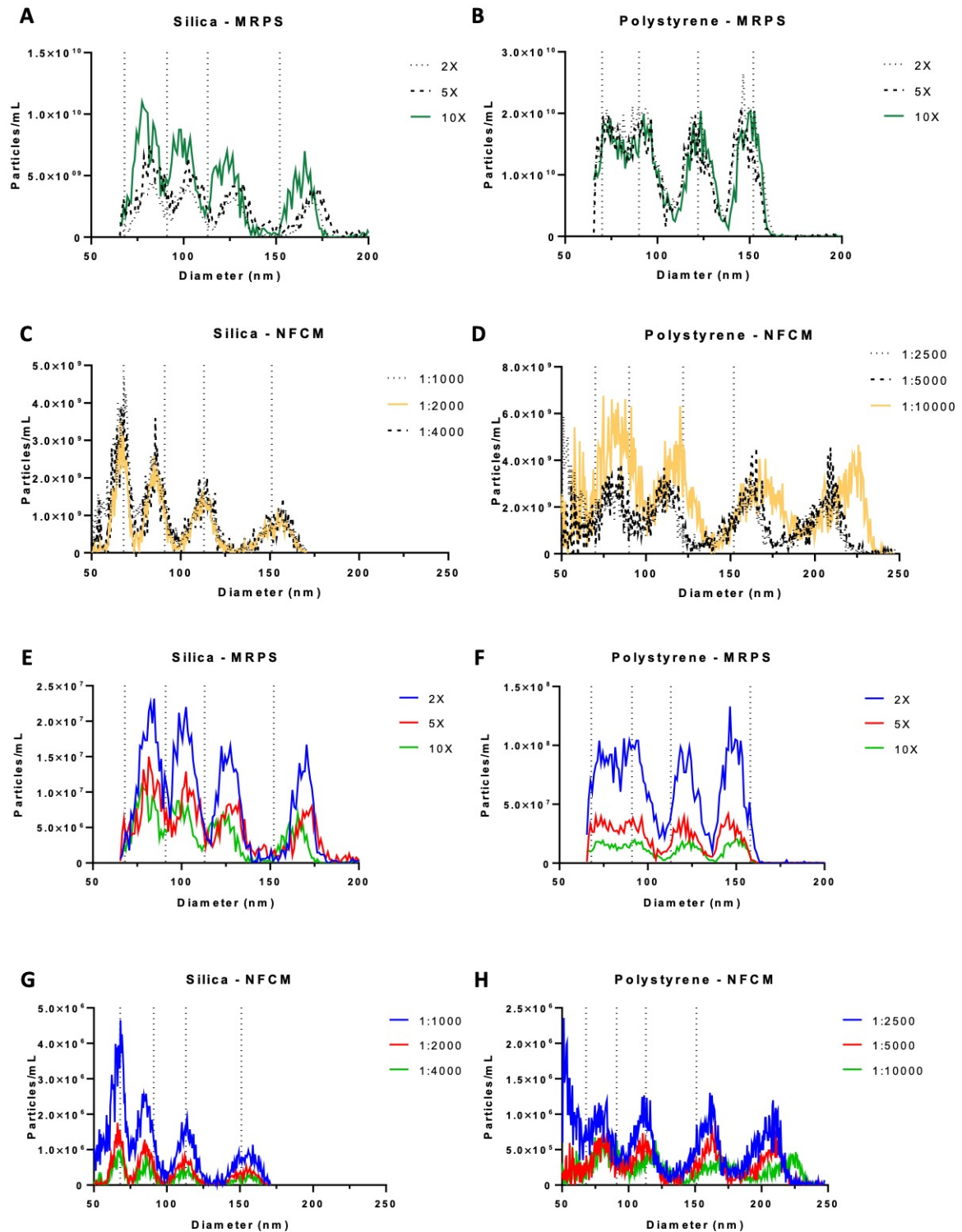
Supplementary Table 1. Antibodies tested with fluorescent NTA

Tetraspanin	Fluorophore	Manufacturer	Catalog Number	Signal
CD81	AF488	Santa Cruz	sc-166029	No
	PE	BD Biosciences	BDB555676	Yes
	PerCP	BD Biosciences	BDB565430	No
	APC	BD Biosciences	BDB561958	No
CD63	AF488	Santa Cruz	sc-5275	No
	AF488	Novus Biologicals	NBP2-42225	No
	PE	AbCam	ab205540	No
	V450	BD Biosciences	BDB561984	No
CD9	PE	BioLegend	312106	No
	PerCP	BD Biosciences	BDB561329	No
	FITC	AbCam	ab34162	No

711